

DOI: 10.1002/cctc.201200891

Photodegradation by a Heterogeneous Mixture of Micro-Sized Anatase and Truncated Rhomboid Anatase Hollow Spheres

Min-Han Yang,^[a] Min-Chiao Tsai,^[a] Yuan-Wei Chang,^[a] Ya-Chen Chang,^[a] Hsin-Tien Chiu,^[b] and Chi-Young Lee*^[a]

Highly uniform hollow spheres were assembled from truncated rhomboid anatase TiO₂ nanoparticles (HS), which were synthesized from the hydrothermal treatment of a NaF solution by using amorphous TiO₂ spheres as a precursor and template. The submicron hollow spheres with highly photocatalytic active surfaces exhibited excellent photocatalytic behavior. In this investigation, the factors that enhanced the photocatalytic performance were examined in terms of light harvesting, photoefficiency, and reaction activity. The photocatalytic performance was increased by a factor of approximately 1.5 for the scattering structure of submicron hollow spheres than that of nanofragments of submicron hollow sphere powder. The rate

constant of anatase TiO₂ with specific photoactive surfaces at {001} and {101} was approximately six times higher than that of randomly exposed TiO₂ particles. Furthermore, a heterogeneous mixture of the submicron hollow spheres and micro-sized anatase TiO₂ (HS@micro-sized TiO₂) prohibited electron-hole recombination in the catalyst during the degradation reaction. The rate constant for the heterojunction system was 3.4 times greater than that of the individual constituents. The rate constant for HS@micro-sized TiO₂ ($k=0.175\text{ min}^{-1}$) was 1.8 times larger than that of commercial P25 ($k=0.099\text{ min}^{-1}$). HS@micro-sized TiO₂ is a promising photocatalytic material.

Introduction

TiO₂ has attracted immense attention because of its unique properties, which include excellent photostability, ecofriendliness, and low cost. It has a wide range of applications in photocatalysis,^[1] dye-sensitized solar cells (DSSCs),^[2] lithium-ion storage,^[3] and electrochromic devices.^[4]


TiO₂ is the most studied photocatalyst because of the high oxidation capacity of its holes. A general photocatalytic procedure involves three main processes: irradiation-induced formation of electrons and holes, bulk diffusion of electrons and holes to the surface, and a surface reaction of the photogenerated carriers with the pollutant. Increasing the light harvesting, reducing the charge recombination, and increasing the surface reactivity are three methods to improve photocatalytic efficiency. To increase light harvesting, TiO₂ has been treated by using a photosensitive material^[5] or doped^[6] to extend its light absorbance into the visible-light region. However, such additional treatment also causes thermal or crystal instability and the trapping of carriers, which considerably reduces efficiency.

However, Mie scattering by a submicron structure increases the average photon path-length,^[7] which markedly increases light harvesting. A hollow sphere structure with a strong scattering effect and high surface area was used to enhance photocatalytic activity.^[8] To reduce the recombination of electrons and holes in the photocatalytic process, heterogeneous structures have been extensively adopted against self-recombination.^[9] Generally, photoexcited electrons are transferred to the interface of the heterogeneous structure, which results in the efficient separation of electrons and holes. Commercial P25 (particles comprised of 75% anatase and 25% rutile) is an effective photocatalyst owing to the synergy between anatase and rutile.^[10] Additionally, our group has reported an excellent photocatalyst that is effective over a wide range of pH values, which was formed by mixing micro- and nano-sized anatases.^[1b] Anatase of different sizes has different flat-band states. Mixing TiO₂ particles with various band positions facilitates the transfer of electrons therein, which results in the separation of electrons and holes and greatly improves the photocatalytic performance. Additionally, the atomic arrangement and Ti coordination at the surface strongly influence the transfer of photoexcited carriers at the surface and the adsorption/desorption between the photocatalyst and the pollutant molecules. Numerous studies have reported that anatase TiO₂ with exposed {001} facets exhibits excellent photocatalytic activity.^[11]

This study attempts to elucidate the details of the photocatalytic reaction. The aforementioned three strategies are used to improve the photocatalytic efficiency. Highly uniform hollow anatase TiO₂ submicron spheres with exposed {001} and {101}

[a] M.-H. Yang, Dr. M.-C. Tsai, Y.-W. Chang, Y.-C. Chang, Prof. C.-Y. Lee
Department of Materials Science and Engineering
National Tsing Hua University
101, Sec. 2, Kuang-Fu Road, Hsinchu 300, Taiwan (R.O. China)
Fax: (+886) 03-5722366
E-mail: cylee@mx.nthu.edu.tw

[b] Prof. H.-T. Chiu
Department of Applied Chemistry
National Chiao Tung University
1001 University Road, Hsinchu 300, Taiwan (R.O. China)

 Supporting information for this article is available on the WWW under <http://dx.doi.org/10.1002/cctc.201200891>.

facets were synthesized and mixed with micro-sized TiO_2 to form a superior photocatalyst.

Results and Discussion

The field emission SEM (FESEM) image of the highly uniform spherical TiO_2 with a mean diameter of 450 nm, which was synthesized by reacting titanium isopropoxide (TTIP) with carboxylic acid, is shown in Figure S1. These spheres are amorphous with solid interiors and smooth surfaces as described in our earlier work.^[7a] Highly uniform hollow anatase TiO_2 spheres were synthesized by using amorphous TiO_2 spheres as a precursor and template by using a hydrothermal process. After hydrothermal treatment with NaF solution (0.15 M), the spheres (ca. 550 nm in diameter) retained their spherical, uniform shape, whereas the smooth surfaces of the precursor spheres became rough (Figure 1A). Furthermore, the solid spheres became hollow after 18 h of hydrothermal treatment (Fig-

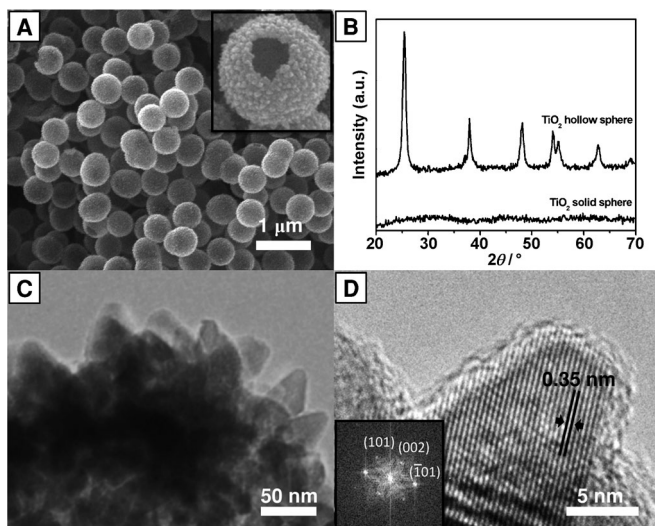


Figure 1. A) FESEM image of hollow spheres following hydrothermal treatment. Inset: image at high magnification. B) Powder XRD pattern of solid and hollow TiO_2 spheres. C) TEM image of hollow spheres with rough surfaces. D) HRTEM image of a truncated rhomboid particle. Inset: Fourier-transformed image.

ure 1A, inset). The XRD pattern shown in Figure 1B reveals that the hollow spheres of TiO_2 with rough surfaces are in a crystalline anatase phase. By using Scherrer's equation, the size of the crystalline anatase particles was estimated to be approximately 13 nm. BET analysis reveals that these hollow spheres have a specific surface area of $83.22 \text{ m}^2 \text{ g}^{-1}$.

A magnified TEM image of the hollow spheres with rough surfaces assembled from truncated rhomboid nanoparticles is shown in Figure 1C. The high-resolution TEM (HRTEM) image shown in Figure 1D reveals that the d spacing is 0.35 nm between the anatase (101) planes and truncated planes {101} and (002), respectively, shown in the Fourier-transformed image inset in Figure 1D. According to the literature, it is believed that the formation mechanism of the TiO_2 hollow

spheres involves a localized Ostwald ripening or chemically induced self-transformation.^[8d,12] The exposure of the {001} surfaces in anatase TiO_2 can be attributed to fluoride ions, which adsorb onto the {001} facets and restrain the crystal growth.^[13] Based on the above findings, anatase TiO_2 hollow spheres were assembled from truncated rhomboids with exposed {101} and {001} surfaces by the hydrothermal method. The {101} and {001} surfaces are generally the most photocatalytically active surfaces of anatase TiO_2 .^[11a,b]

These TiO_2 submicron-sized hollow spheres (HS) with high specific surface areas, assembled from anatase nanoparticles with exposed {101} and {001} surfaces exhibit good photocatalytic behavior, and the degradation rate constant of methylene blue under irradiation by an Xe lamp is approximately 0.080 min^{-1} . The superior photocatalytic properties of these particles were further examined.

Effect of the scattering structure of TiO_2 on the photocatalytic performance

According to Mie scattering theory, uniform submicron spheres can scatter light at a particular wavelength,^[14] which increases the mean photon path-length. The UV/Vis spectra of HS and the nanofragments (NF) are presented in Figure 2A, which show the absorbance of the TiO_2 band edge. In addition, the spectrum of HS from 400–900 nm shows a clear wave shape (Figure 2A, inset). The waveform can be regarded as the superposition of the TiO_2 band edge and the Mie scattering wave. Moreover, a distinct oblique shape is observed between 300 and 350 nm in the UV/Vis spectrum of HS, which is also a contribution of the Mie scattering of the hollow sphere structure. Thus, HS was expected to exhibit a good photocatalytic performance. The photocatalytic behavior of HS and NF in the degradation of methylene blue under irradiation by a Xe lamp are shown in Figure 2B. The reaction was a first-order reaction, and the rate constants (k) of the degradation reaction using HS and NF as photocatalysts are 0.080 and 0.053 min^{-1} , respectively. HS and NF had the same specific surface area and microstructure. As HS had a submicron sphere structure, the scattering of light from the submicron spheres increases the average photon path-length, which results in increased light harvesting and significantly improves the photocatalytic performance.

Effect of exposing the surfaces of TiO_2 on the photocatalytic performance

To study the effect of the exposure of particular planes of TiO_2 on the photocatalytic performance, anatase TiO_2 nanoparticles with randomly exposed surfaces were synthesized by the hydrothermal treatment of amorphous TiO_2 with deionized (DI) water in the absence of NaF followed by crushing. The TEM images presented in Figure 3A and B show that the anatase TiO_2 NF with exposed {001} and {101} planes has particular exposed surfaces and larger grains than that of irregular TiO_2 particles. The crushed powder of randomly exposed TiO_2 particles with a high specific surface area ($132.96 \text{ m}^2 \text{ g}^{-1}$) was expected to exhibit a good photocatalytic performance. However, the

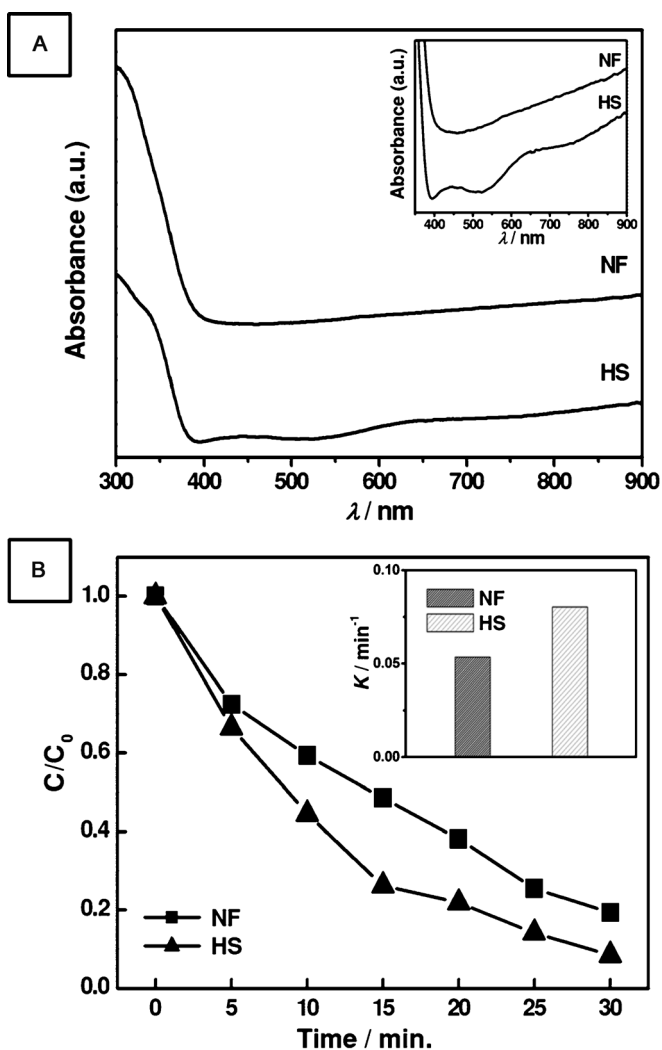


Figure 2. A) UV/Vis spectra of HS and NF. B) Photocatalytic performance of HS and NF in the degradation of methylene blue under irradiation by Xe lamp. Inset: rate constant of degradation of methylene blue using HS and NF.

photocatalytic performance of randomly exposed TiO_2 particles ($k=0.009 \text{ min}^{-1}$) was not as good as that of particles with exposed {101} and {001} surfaces ($k=0.053 \text{ min}^{-1}$; Figure 3C and D). Many research groups have demonstrated that TiO_2 particles with exposed {001} surfaces have the best photocatalytic behavior, and TiO_2 with exposed {001} and {101} planes has a higher photocatalytic performance than that of pure {101}-exposed TiO_2 .^[11a,b] From our observations, even though the surface area of the randomly exposed particles ($132.96 \text{ m}^2 \text{ g}^{-1}$) greatly exceeded that of {001}- and {101}-exposed anatase ($83.22 \text{ m}^2 \text{ g}^{-1}$), {001}- and {101}-exposed anatase shows a superior photocatalytic behavior to that of the randomly exposed particles. The high crystallinity and the large amount of {001}- and {101}-exposed active sites of NF enhances the photocatalytic behavior compared to that of the randomly exposed particles.

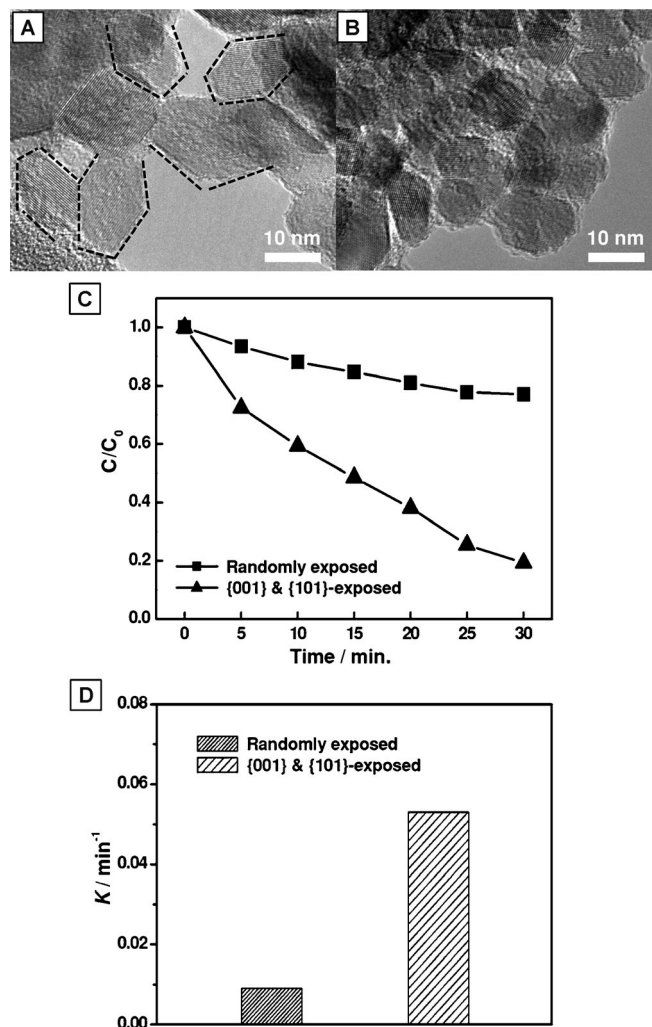


Figure 3. TEM images of A) NF with exposed {101} and {001} surfaces, and B) randomly exposed particles hydrothermally treated without NaF. C) Photocatalytic performance of NF and randomly exposed particles. D) Rate constant of the degradation of methylene blue using NF and randomly exposed particles.

Photocatalytic performance of a mixed system of TiO_2

Based on the above observations, HS with a high specific surface area, a structure that supports Mie scattering, and a large exposed reactive surface area exhibits the strongest photocatalytic performance of various titanium dioxides. However, the performance of HS is close to that of commercial P25 (Figure 4A). P25 comprises 75% anatase and 25% rutile, which exhibit a synergetic effect. The close contact between anatase and rutile effectively separates the electrons from the holes and reduces the recombination, which considerably improves the photocatalytic performance.^[9c,10] In our earlier investigation,^[1b] not only the use of different phases of the material but also the mixing of differently sized anatase TiO_2 exhibits improved the photocatalytic performance. Differently sized materials with different flat bands and opposite zeta potentials attract each other, which results in electron hopping among the particles and reduces electron-hole recombination to greatly

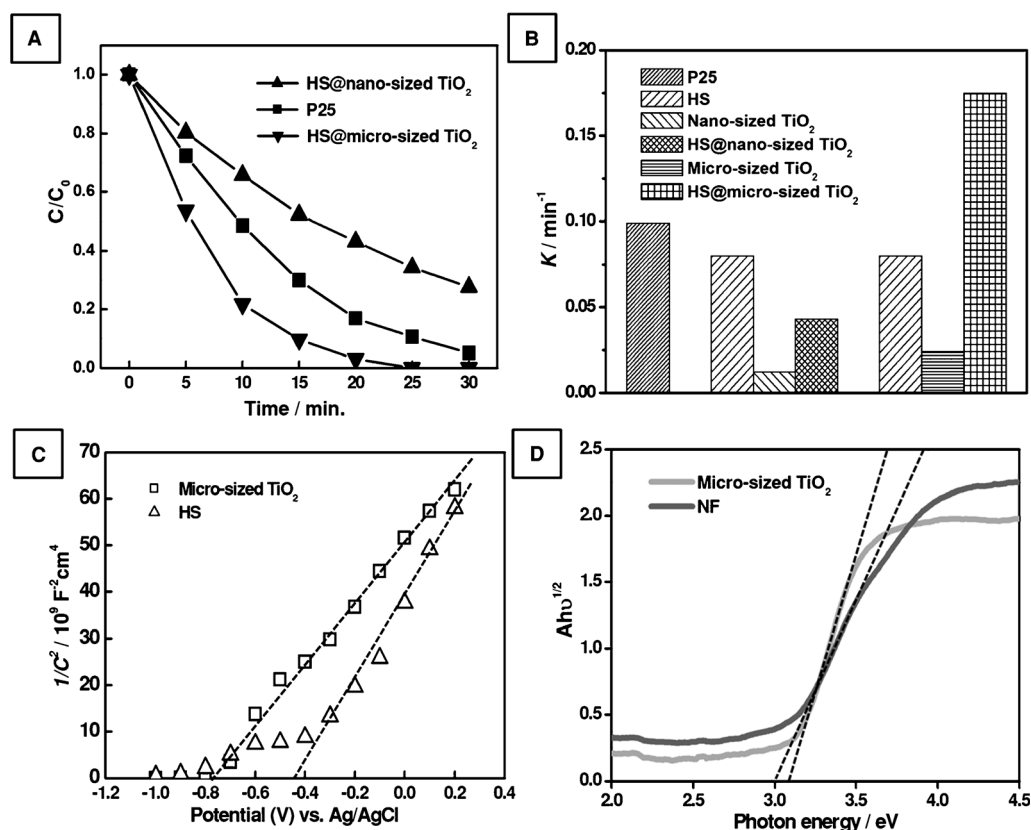


Figure 4. A) Photocatalytic performance of HS@micro-sized TiO₂, HS@nano-sized TiO₂, and P25. B) Comparison of rate constants of the degradation of methylene blue using TiO₂. C) Mott–Schottky plots for NF and micro-sized TiO₂ electrodes in 1 M NaCl (with Ag/AgCl reference electrode). D) Plots of modified Kubelka–Munk function against the energy of light absorbed by NF and micro-sized TiO₂.

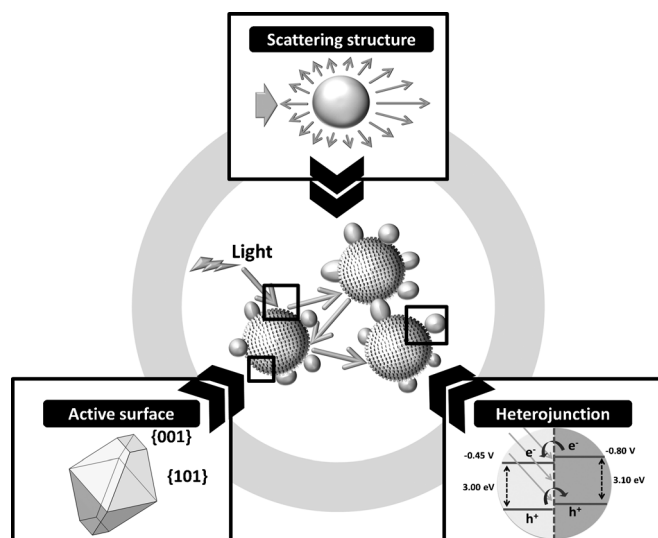
improve the photocatalytic performance. Therefore, micro- and nano-sized TiO₂ was introduced into HS to form a heterogeneous composite of HS@micro-sized TiO₂ and HS@nano-sized TiO₂ to inhibit electron–hole recombination. Micro- and nano-sized TiO₂ each exhibit a very poor photocatalytic performance (Figure S2). Even though the nano-sized TiO₂ has a large surface area, the rate constants for the degradation of methylene blue using micro- and nano-sized TiO₂ are 0.024 and 0.012 min⁻¹, respectively. The rate constants of the degradation of methylene blue using the heterojunction systems HS@micro-sized TiO₂ and HS@nano-sized TiO₂ are 0.175 min⁻¹ and 0.043 min⁻¹, respectively. The photocatalytic performance of HS@micro-sized TiO₂ ($k=0.175\text{ min}^{-1}$) is far better than that of the individual HS ($k=0.080\text{ min}^{-1}$) and micro-sized TiO₂ ($k=0.024\text{ min}^{-1}$). The rate constant of the heterojunction system is 3.4 times greater than that of the individual HS and micro-sized TiO₂ ($k=0.080\times 50\%+0.024\times 50\%=0.052\text{ min}^{-1}$). Furthermore, the degradation rate constant of methylene blue using HS@micro-sized TiO₂ is 1.8 times larger than that of commercial P25 ($k=0.099\text{ min}^{-1}$; Figure 4B). However, HS@nano-sized TiO₂ still exhibits a poor photocatalytic behavior, which suggests that perhaps the heterojunction structure cannot be constructed by using the mixed system.

From the zeta potentials, the surface charges on HS, nano-sized TiO₂, and micro-sized TiO₂ are +10, +3.5, and -44 mV, respectively. HS and nano-sized TiO₂ have a positive surface

charge, whereas micro-sized TiO₂ has a negative surface charge. Thus, HS and micro-sized TiO₂ attract each other, whereas HS and nano-sized TiO₂ repel each other.^[15] To obtain the band diagrams of HS and the micro-sized TiO₂ system, the flat-band potentials and band gaps were evaluated. The flat-band potentials were determined from the Mott–Schottky plots^[1b,16] of HS and micro-sized TiO₂ as -0.45 and -0.80 V, respectively (Figure 4C). The band gaps estimated from the plots of the modified Kubelka–Munk function against the energy of light absorbed are 3.00 and 3.10 eV for NF and micro-sized TiO₂, respectively (Figure 4D).^[17] Herein, a type II semiconductor heterojunction system was established (Scheme 1). The type II model is extensively used in photocatalytic systems to explain the decrease in electron–hole recombination.^[18] In this work, a heterojunction system was constructed by mixing HS and micro-sized TiO₂ to reduce electron–hole recombination. The surviving holes can oxidize the target pollutant directly^[19] or react with OH⁻ to generate OH[•] to oxidize the target,^[20] which leads to the remarkable photocatalytic oxidation reaction.^[21]

Conclusions

A mixture of micro-sized anatase TiO₂ and submicron hollow spheres assembled from truncated rhomboid TiO₂ nanoparticles, HS@micro-sized TiO₂, exhibits a better photocatalytic per-



Scheme 1. Factors that dominate photocatalytic performance are light harvesting, photoefficiency, and the reaction activity of TiO_2 .

formance than commercial P25. The significant advantages of HS@micro-sized TiO_2 are the high scattering efficiency of its submicron spherical structure, the exposure of active surfaces, its high crystallinity, and the heterojunction structure (Scheme 1). Firstly, the submicron spherical structure of TiO_2 scattered UV light, which increased the light path-length and increased light harvesting. The rate constant of methylene blue degradation using hollow sphere anatase TiO_2 was 1.5 times larger than that using the nanofragments. Secondly, the hollow spheres were assembled as truncated rhomboid nanoparticles with exposed {001} and {101} planes. Although the surface area of the {001}- and {101}-exposed anatase ($83.22 \text{ m}^2 \text{ g}^{-1}$) was less than that of randomly exposed particles ($132.96 \text{ m}^2 \text{ g}^{-1}$), the rate constant of methylene blue degradation using the {001}- and {101}-exposed truncated rhomboid anatase was approximately six times greater than that of particles with randomly exposed planes. Finally, to further improve the photocatalytic performance, the mixed system was introduced to prohibit electron-hole recombination in the catalyst. The heterogeneous environment was obtained from differently sized materials with different flat bands and opposite zeta potentials. The rate constant of the heterojunction system HS@micro-sized TiO_2 is 3.4 times greater than that of the individual materials. The reaction rate constant of HS@micro-sized TiO_2 ($k=0.175 \text{ min}^{-1}$) is 1.8 times larger than that of commercial P25 ($k=0.099 \text{ min}^{-1}$). The method described here may be applied to photoelectron conversion, such as in the degradation of organic pollutants, water splitting, and DSSCs.

Experimental Section

Preparation of hollow anatase TiO_2 spheres

Hollow anatase TiO_2 spheres (HS) were formed by using the following hydrothermal process. Amorphous TiO_2 solid spheres (2 g), which we synthesized previously,^[7a] were dispersed in aqueous NaF

(0.15 M). This precursor solution was transferred into a Teflon-lined autoclave and heated to 190°C for 18 h. After the hydrothermal reaction, the products were washed with DI water and dried at 50°C .

Material characterization

FESEM (JSE-6500F) was used to characterize the surface morphologies of the anatase TiO_2 materials. The morphology and microstructure of the anatase TiO_2 were examined by using HRTEM (JEOL 2010). Phase detection was performed by using powder XRD (Bruker D8-advanced) using $\text{Cu-K}\alpha$ radiation ($\lambda=1.5405981 \text{ \AA}$). The optical behavior of the materials was determined by using UV/Vis spectroscopy (AvaSpec-2048UVspectrum). The flat-band potentials were measured by using an electrochemical instrument (AUTOLAB, PGSTAT30) in 1 M NaCl at 100 Hz. The Mott-Schottky curves were plotted with the square of the inverse capacity as the ordinate and voltage as the abscissa. The flat-band potentials were determined from the intercepts with the abscissa.

Photocatalytic experiments

Anatase TiO_2 was used for all photocatalytic experiments. Irradiation was performed by using a 180 W Xe lamp (Osram), and the temperature was maintained at 296 K by using a water cooling-jacket. The target pollutant was methylene blue. Catalyst powder (0.01 g) was dispersed to a concentration of 25 ppm in methylene blue solution. After the absorption had stabilized, the solution was illuminated from the top with magnetic stirring. Samples (1 mL) were removed every 5 min, filtered through $0.2 \mu\text{m}$ filter, and diluted with DI water (1.5 mL). The filtrate was analyzed by using UV/Vis spectroscopy (AvaSpec-2048 UV spectrum) to determine the concentration of methylene blue. To elucidate the effect of the submicron-sphere structure of HS on light scattering, nanofragments of HS powder (NF) were used as reference samples. Furthermore, the effect of the exposed active surface of the TiO_2 was illustrated by using randomly exposed anatase TiO_2 powder as reference samples. HS and commercial micro-sized (Riedel-de Haen) or nano-sized (Alfa Aesar) particles were mixed in a 1:1 ratio (0.005 g each) to elucidate the mixing system. HS mixed with micro-sized TiO_2 or nano-sized TiO_2 is referred to as HS@micro-sized TiO_2 and HS@nano-sized TiO_2 , respectively. The photocatalytic reaction exhibited first-order behavior, and the pseudo-first-order rate constant (k) was calculated by using the equation $k = -[\ln(C/C_0)]/\Delta t$, in which C and C_0 represent the final and initial concentrations, respectively, and Δt is time.

Acknowledgements

The authors would like to thank the National Science Council of the Republic of China, Taiwan, for financially supporting this research under contract No. NSC 99-2113M-007-011.

Keywords: environmental chemistry · titanium · dyes/pigments · nanoparticles · photochemistry

[1] a) T. Y. Ke, C. W. Peng, C. Y. Lee, H. T. Chiu, H. S. Sheu, *CrystEngComm* **2009**, *11*, 1691–1695; b) T.-Y. Ke, C.-Y. Lee, H.-T. Chiu, *Appl. Catal. A* **2010**, *381*, 109–113.

[2] a) B. O'Regan, M. Grätzel, *Nature* **1991**, *353*, 737–740; b) A. Yella, H. W. Lee, H. N. Tsao, C. Y. Yi, A. K. Chandiran, M. K. Nazeeruddin, E. W. G. Diau, C. Y. Yeh, S. M. Zakeeruddin, M. Grätzel, *Science* **2011**, *334*, 629–634.

- [3] a) M. C. Tsai, J. C. Chang, H. S. Sheu, H. T. Chiu, C. Y. Lee, *Chem. Mater.* **2009**, *21*, 499–505; b) P.-C. Chen, M.-C. Tsai, H.-C. Chen, I. N. Lin, H.-S. Sheu, Y.-S. Lin, J.-G. Duh, H.-T. Chiu, C.-Y. Lee, *J. Mater. Chem.* **2012**, *22*, 5349–5355.
- [4] a) A. Ghicov, M. Yamamoto, P. Schmuki, *Angew. Chem.* **2008**, *120*, 8052–8055; *Angew. Chem. Int. Ed.* **2008**, *47*, 7934–7937; b) M. H. Yang, T. T. Chen, Y. S. Wang, H. T. Chiu, C. Y. Lee, *J. Mater. Chem.* **2011**, *21*, 18738–18743.
- [5] a) S. C. Lo, C. F. Lin, C. H. Wu, P. H. Hsieh, *J. Hazard. Mater.* **2004**, *114*, 183–190; b) L. Huang, F. Peng, H. J. Wang, H. Yu, Z. Li, *Catal. Commun.* **2009**, *10*, 1839–1843.
- [6] a) R. Asahi, T. Morikawa, T. Ohwaki, K. Aoki, Y. Taga, *Science* **2001**, *293*, 269–271; b) J. Wang, D. N. Tafen, J. P. Lewis, Z. Hong, A. Manivannan, M. Zhi, M. Li, N. Wu, *J. Am. Chem. Soc.* **2009**, *131*, 12290–12297.
- [7] a) M. C. Tsai, T. L. Tsai, C. T. Lin, R. J. Chung, H. S. Sheu, H. T. Chiu, C. Y. Lee, *J. Phys. Chem. C* **2008**, *112*, 2697–2702; b) K. Awazu, M. Fujimaki, C. Rockstuhl, J. Tominaga, H. Murakami, Y. Ohki, N. Yoshida, T. Watanabe, *J. Am. Chem. Soc.* **2008**, *130*, 1676–1680; c) L. Zhang, H. Wang, *J. Phys. Chem. C* **2011**, *115*, 18479–18485.
- [8] a) J. Yu, S. Liu, H. Yu, *J. Catal.* **2007**, *249*, 59–66; b) J. Yu, H. Yu, H. Guo, M. Li, S. Mann, *Small* **2008**, *4*, 87–91; c) X. Yu, J. Yu, B. Cheng, B. Huang, *Chem. Eur. J.* **2009**, *15*, 6731–6739; d) J. Yu, J. Zhang, *Dalton Trans.* **2010**, *39*, 5860–5867.
- [9] a) Y. Cao, X. T. Zhang, W. S. Yang, H. Du, Y. B. Bai, T. J. Li, J. N. Yao, *Chem. Mater.* **2000**, *12*, 3445–3448; b) T. Ohno, K. Tokieda, S. Higashida, M. Matsumura, *Appl. Catal. A* **2003**, *244*, 383–391; c) R. G. Nair, S. Paul, S. K. Samdarshi, *Sol. Energy Mater. Sol. Cells* **2011**, *95*, 1901–1907.
- [10] a) R. I. Bickley, T. Gonzalezcarreno, J. S. Lees, L. Palmisano, R. J. D. Tilley, *J. Solid State Chem.* **1991**, *92*, 178–190; b) D. C. Hurum, A. G. Agrios, K. A. Gray, T. Rajh, M. C. Thurnauer, *J. Phys. Chem. B* **2003**, *107*, 4545–4549.
- [11] a) H. G. Yang, G. Liu, S. Z. Qiao, C. H. Sun, Y. G. Jin, S. C. Smith, J. Zou, H. M. Cheng, G. Q. Lu, *J. Am. Chem. Soc.* **2009**, *131*, 4078–4083; b) D. Q. Zhang, G. S. Li, X. F. Yang, J. C. Yu, *Chem. Commun.* **2009**, 4381–4383; c) Z. K. Zheng, B. B. Huang, J. B. Lu, X. Y. Qin, X. Y. Zhang, Y. Dai, *Chem. Eur. J.* **2011**, *17*, 15032–15038.
- [12] H. G. Yang, H. C. Zeng, *J. Phys. Chem. B* **2004**, *108*, 3492–3495.
- [13] a) H. G. Yang, C. H. Sun, S. Z. Qiao, J. Zou, G. Liu, S. C. Smith, H. M. Cheng, G. Q. Lu, *Nature* **2008**, *453*, 638–U634; b) S. Liu, J. Yu, M. Jaroniec, *J. Am. Chem. Soc.* **2010**, *132*, 11914–11916.
- [14] a) A. Ashkin, J. M. Dziedzic, *Appl. Opt.* **1981**, *20*, 1803–1814; b) C. B. Richardson, R. L. Hightower, A. L. Pigg, *Appl. Opt.* **1986**, *25*, 1226–1229; c) M. L. Breen, A. D. Dinsmore, R. H. Pink, S. B. Qadri, B. R. Ratna, *Langmuir* **2001**, *17*, 903–907.
- [15] F. Xiao, F. Wang, X. Fu, Y. Zheng, *J. Mater. Chem.* **2012**, *22*, 2868–2877.
- [16] C. Baumanis, D. W. Bahnemann, *J. Phys. Chem. C* **2008**, *112*, 19097–19101.
- [17] a) S. Sakthivel, M. Janczarek, H. Kisch, *J. Phys. Chem. B* **2004**, *108*, 19384–19387; b) T. A. Kandiel, A. Feldhoff, L. Robben, R. Dillert, D. W. Bahnemann, *Chem. Mater.* **2010**, *22*, 2050–2060.
- [18] a) W. T. Sun, Y. Yu, H. Y. Pan, X. F. Gao, Q. Chen, L. M. Peng, *J. Am. Chem. Soc.* **2008**, *130*, 1124–1125; b) R. Brahimi, Y. Bessekhoud, A. Bouguelia, M. Trari, *J. Photochem. Photobiol. A* **2008**, *194*, 173–180.
- [19] H. Lu, J. Zhao, L. Li, L. Gong, J. Zheng, L. Zhang, Z. Wang, J. Zhang, Z. Zhu, *Energy Environ. Sci.* **2011**, *4*, 3384–3388.
- [20] Q. Xiang, J. Yu, P. K. Wong, *J. Colloid Interface Sci.* **2011**, *357*, 163–167.
- [21] W. Y. Teoh, J. A. Scott, R. Amal, *J. Phys. Chem. Lett.* **2012**, *3*, 629–639.

Received: December 2, 2012

Revised: February 28, 2013

Published online on May 22, 2013